NASA Technical Paper 1574

Experimental Determination of Position-Estimate Accuracy Using Back-Azimuth Signals From a Microwave Landing System

Charles E. Knox

DECEMBER 1979

NASA

NASA Technical Paper 1574

Experimental Determination of Position-Estimate Accuracy Using Back-Azimuth Signals From a Microwave Landing System

Charles E. Knox
Langley Research Center
Hampton, Virginia

National Aeronautics
and Space Administration

**Scientific and Technical
Information Branch**

1979

SUMMARY

Flight tests with the NASA Terminal Configured Vehicle (TCV) Boeing 737 were made to investigate the use of back-azimuth signals to estimate airplane position. Position estimates were established by three update methods: a combination of microwave landing system (MLS) back-azimuth and distance-measuring-equipment (DME) signals, MLS back-azimuth signals alone, and dual DME signals. Position-estimate error was obtained by comparison of the position estimate from the airplane navigation system with the tracking information from a ground-based radar system.

The results of these tests showed that the most accurate position estimates were obtained with a combination of back-azimuth and DME signals. The next most accurate estimates were made with only back-azimuth signals. Of the three update modes tested, the least accurate estimates were made with dual DME signals.

Analysis of the position-estimate error data showed that the component of error due to the DME signal input was larger than the component due to the MLS back-azimuth signal input. The use of a precision DME signal input would be expected to reduce position-estimate error.

INTRODUCTION

The NASA Terminal Configured Vehicle (TCV) previously demonstrated the ability to navigate along a curved path approach to landing (ref. 1) with an onboard navigation system utilizing position information from the time-referenced scanning-beam (TRSB) microwave landing system (MLS). During operations in the MLS environment, azimuth and elevation-angle information was obtained from two scanning beams, and distance information was provided by MLS precision distance-measuring equipment (PDME) for use in the onboard navigation and automatic landing systems. The TRSB MLS provides azimuth information within 60° of each side of the runway center line, elevation-angle information up to 20°, and PDME range information up to 37 040 m (20 n. mi.) from the MLS antennas.

Missed-approach navigation capability was available from the MLS system in the form of back-azimuth and PDME information. Hence, to fully utilize the TRSB MLS, algorithms using back-azimuth information were incorporated into the TCV airplane navigation computer for use in generating missed-approach guidance. Flight tests then were conducted to determine the navigation accuracy from MLS back-azimuth signals.

The purpose of this report is to describe the equations and logic used to generate a navigation position estimate in the MLS back-azimuth signal environment and to document the error in the navigation position estimate. The equations described are used to calculate position difference components from (1) MLS back-azimuth bearing and range information from arbitrarily located

DME stations, and (2) MLS back-azimuth bearing information alone. A summary of the TCV position-estimate update process is also described. The navigation position-estimate error calculated from flight data and radar tracking information is analyzed to determine the relative errors due to DME and back-azimuth signal inputs. The position-estimate error data using the MLS inputs are also compared with error data obtained during dual DME updates, the primary position-estimate mode.

SYMBOLS

A	distance between the DME and MLS back-azimuth antenna, n. mi.
a	east component of A, n. mi.
b	north component of A, n. mi.
D	distance from DME to airplane corrected for slant range, n. mi.
D'	slant range distance from DME to airplane, n. mi.
$\overrightarrow{DP}$	position difference vector
$\overrightarrow{DP}_p$	component of position difference vector $\overrightarrow{DP}$ perpendicular to the runway center line
DP_p	magnitude of vector $\overrightarrow{DP}_p$, n. mi.
e_p	magnitude of the component of position-estimate error perpendicular to the back-azimuth bearing on which the airplane is located, m
e_R	magnitude of the component of position-estimate error parallel to the back-azimuth bearing on which the airplane is located, m
e_θ	azimuth bearing-error angle, deg
F	ellipticity constant, 0.003367
$h_{a/p}$	altitude of airplane above mean sea level, m
h_{DME}	altitude of DME antenna above mean sea level, m
h_o	altitude of MLS back-azimuth antenna above mean sea level, m
$\hat{i},\hat{j}$	unit coordinate vectors
K_1	position update gain
K_2	velocity update gain, sec^{-1}
L	outer radial limit of back-azimuth volumetric check, m (n. mi.)

M inner radial limit of back-azimuth volumetric check, m

N,E axes of orthogonal coordinate system oriented toward true north

P angle formed by the vector $\vec{Z}_m$ and a line between the airplane and DME antenna, deg

R range from the back-azimuth antenna to the airplane, m

r_E radius of Earth, m

r_M meridional radius of curvature, m

r_N normal radius of curvature, m

$\hat{u}$ unit vector perpendicular to the runway center line

V_N,V_E north, east components of navigation system velocity estimate, knots

$\hat{V}_N,\hat{V}_E$ north, east components of inertial ground speed, knots

X',Y' axes of orthogonal coordinate system oriented along the runway center line

X'_e,Y'_e coordinates of vector $\vec{Z}_e$ transformed into the X',Y' coordinate system

$\vec{Z}_e$ vector of airplane estimated position from the MLS back-azimuth antenna

Z_e magnitude of $\vec{Z}_e$, n. mi.

$Z_{e,N},Z_{e,E}$ north, east components of $\vec{Z}_e$, n. mi.

$\vec{Z}_m$ vector of airplane measured position from the MLS back-azimuth antenna

Z_m magnitude of $\vec{Z}_m$, n. mi.

$Z_{m,N},Z_{m,E}$ north, east components of $\vec{Z}_m$, n. mi.

$\vec{Z}_r$ vector of airplane position estimated radially along the measured azimuth angle

Z_r magnitude of position vector Z_r, n. mi.

$Z_{r,N},Z_{r,E}$ north, east components of position vector $\vec{Z}_r$, n. mi.

α angle formed at the back-azimuth antenna by the DME antenna and the measured airplane position, deg

$\Delta P_N,\Delta P_E$ north, east components of position-estimate error, n. mi.

Δt change in time

$\Delta V_N, \Delta V_E$ north, east components of system velocity update, knots

$\Delta\phi, \Delta\lambda$ latitude, longitude update estimates

η back-azimuth angle relative to the runway center line, deg

μ relative angle between the DME and the MLS back-azimuth antenna, deg

$\phi_{DME}, \lambda_{DME}$ latitude, longitude of DME antenna location, deg

ϕ_e, λ_e latitude, longitude of airplane position estimate, deg

ϕ_o, λ_o latitude, longitude of back-azimuth antenna location, deg

ψ_r runway heading to true north, deg

Ω vertical angular limit of back-azimuth volumetric check, deg

ω lateral angular limit of back-azimuth volumetric check, deg

Subscripts:

t at time t

t-1 at iteration time previous to time t

Abbreviations:

DME distance-measuring equipment

IBD navigation update mode: inertial velocity, back azimuth and DME

IBX navigation update mode: inertial velocity, back azimuth alone

IDD navigation update mode: inertial velocity, dual DME

MLS microwave landing system

NCU navigation computer unit

PDME precision distance-measuring equipment

VOR very-high-frequency omnidirectional-range ratio

AIRPLANE, EXPERIMENTAL SYSTEMS, AND EQUIPMENT

Airplane

The NASA test airplane is the Boeing 737-100 twin-jet transport airplane shown in figure 1. The TCV airplane is used as a research vehicle with separate experimental navigation, guidance, flight control, and display systems located in a separate research cockpit. All of the normal flight systems (flight control, navigation, pressurization, etc.) have been retained in the conventional cockpit in a normal, functional state. This arrangement allows changes to be made to any of the experimental systems while retaining the standard operational features of the airplane.

Experimental Systems

The experimental research flight systems consist of a triplex digital flight control computer system, an electronic cathode-ray-tube (CRT) display system, and a digital navigation and guidance system (ref. 2) integrated into a separate, two-man-crew, research cockpit. Figure 2 is a simplified functional block diagram of the navigation, guidance, and control process during automatic path tracking (ref. 3). The navigation and guidance calculations are performed in a single digital navigation computer. Various navigation sensor signals (including inertial-navigation-system velocities and accelerations, true airspeed, magnetic heading, and MLS back-azimuth, VOR, and DME radio signals) are used in the navigation computer. This computer estimates the airplane position based on combinations of the sensor inputs. Horizontal path, vertical path, and thrust commands based on the estimated position, velocity, and path tracking errors of the airplane are computed and transferred to the flight control computer system 20 times per second. The flight control system then commands the flight control-surface servos.

Airborne Data Acquisition System

A wide-band magnetic tape recorder onboard the airplane recorded data at a rate of 40 samples per second. These data included 93 parameters describing the airplane configuration, attitude, and control-surface activity. Thirty-two additional channels were used for recording parameters, including the latitude and longitude of the navigation position estimate which was calculated by the navigation computer. Video recordings of the electronic attitude-director and electronic horizontal-situation displays were also made throughout the flights.

Radar Tracking Facilities

Radar tracking of the airplane was provided by the Federal Aviation Administration Extended Area Instrumentation Radar (EAIR) Facility at the National Aviation Facilities Experimental Center (NAFEC) in Atlantic City, New Jersey. The tracking radar is a precision, C-band, instrumentation radar system which was operated in a secondary (beacon-tracking) mode during

these flight tests. Slant range, azimuth angle, and elevation angle data were recorded at a 10-Hz sample rate on magnetic tape. All airborne and ground-based recorded data were time correlated for post-flight processing and analysis. Post-flight processing of the range, azimuth, and elevation data consisted of conversion to latitude, longitude, and altitude.

Radar accuracy, root mean square (rms), is stated (ref. 4) as 0.15 mrad, 5.6 m at 37 040 m (20 n. mi.) in azimuth and elevation and 6 m in range.

MLS and DME

The MLS used during these flight tests was a test bed system oriented for approaches to runway 31 at NAFEC. This system was a time-referenced scanning-beam system with a front-azimuth beam width of 1°, a lateral sweep angle of $\pm 60^{\circ}$, and nominal vertical coverage up to 20°. The glide slope beam was 1° wide and had an azimuthal coverage of approximately $\pm 60^{\circ}$. An MLS PDME with omnidirectional coverage of approximately 37 040 m (20 n. mi.) was used in conjunction with the front-azimuth signals. The back-azimuth beam was 3° wide and had a lateral sweep angle of $\pm 40^{\circ}$. Vertical coverage was between 1° and 20°.

The Atlantic City DME, normally used for en route navigation, was used during the back-azimuth flight testing. This DME is located at the airport 1671 m past the back-azimuth antenna and 229 m left of the runway center line (fig. 3).

When the navigation system updated its position estimate with dual DME, the Atlantic City DME was always used in conjunction with other DME in the area. The navigation system automatically selected, tuned, and checked the validity of the other DME on the basis of strength of signal and station location geometric characteristics so that good position estimates resulted. These geometric characteristics are described in reference 2.

Switching Logic of Airborne MLS Receiver Antenna

The TCV airplane was equipped with two MLS receiver antennas to ensure that the greatest possible signal strength was delivered to the MLS receiver regardless of the airplane direction of flight, its attitude, or its position within the MLS signal coverage. The forward antenna was located on top of the fuselage just above the forward cockpit. The rear antenna was mounted on the bottom of the fuselage below the airplane tail. The MLS airborne receiver contained the logic to determine which antenna was providing the greatest signal strength. The receiver sent a pair of discrete logic signals to an external antenna switch to select the appropriate antenna.

Additional hardware logic in the flight control computers forced selection of the forward antenna while operating in the MLS front-course signal coverage, regardless of the relative signal strengths at the forward and aft antennas. This additional antenna-selection logic was required because the flight control computers did not have the necessary software for antenna switching.

EXPERIMENT DESIGN AND PROCEDURES

The objective of this flight experiment was to determine the accuracy of the navigation position estimate when updated with dual DME signals, with MLS back-azimuth signals, and with a combination of MLS back-azimuth and DME signals. The flight and radar data obtained during these tests were used to compare the accuracies of these update modes and to determine the relative errors due to DME and back-azimuth signal inputs.

The position-estimate error was determined by calculating the vector between the estimated position of the airplane and its position as tracked by ground-based radar (ref. 5). The magnitude of this error vector is the position-estimate error. The mean and standard deviation of the navigation position-estimate error was calculated and used for comparison of the three update modes.

The NASA TCV airplane was flown along three, three-dimensional flight paths (fig. 3), each stored in the navigation data base in the navigation computer. Path 1 was a 5556-m (3-n. mi.) downwind leg with a 180°, descending left turn to a 5556-m (3-n. mi.) final approach to the runway. This path was in the MLS front-course signal coverage and allowed the navigation computer to update its position estimate with the front-course signals just before each test run.

Paths 2 and 3 provided experience with guidance in the area of back-azimuth signal coverage. These paths overlaid the last 5556 m (3 n. mi.) of path 1 so that lateral guidance would be continuous during the transition from front-course to back-course guidance. Path 2 extended 18 520 m (10 n. mi.) from the runway threshold, straight out along the runway center line. Path 3 followed the runway center line for approximately 6482 m (3.5 n. mi.), then made a 45° left turn, and continued an additional 21 298 m (11.5 n. mi.).

Each test run was started with the pilots flying an instrument approach to the runway via path 1. Instead of landing, a missed approach was executed, and the airplane was flown in the MLS back-azimuth coverage along either path 2 or path 3. Upon reaching the end of either of these paths, the airplane was returned to the beginning of path 1 for another test run.

The radar was calibrated with the airplane on a known ground test point. The radar tracked the airplane continuously during the flight from take-off to landing.

DESCRIPTION OF NAVIGATION POSITION ESTIMATE

Position Difference

The TCV navigation computer was programmed to select and tune two appropriate DME and/or VOR stations in the vicinity of the airplane. The distance and/or azimuth information received from these stations was used to update the previous position estimate. This position difference was divided into north ($\Delta P_{N,t}$) and east ($\Delta P_{E,t}$) components to be used in determining new posi-

tion and velocity estimates. The dual DME update mode, the primary position-estimate difference mode, was displayed as IDD on the electronic map displays for each of the flight crews.

Other sources of navigation information could also be used to determine position differences. While operating in the MLS back-azimuth signal coverage, these position-update components were calculated with back-azimuth and DME information. This update mode was shown on the pilots' electronic map display as IBD (inertial velocity, back azimuth, DME). If no DME was available, the estimate mode was IBX (inertial velocity, back azimuth alone). In subsequent sections, the equations used in the IBD and IBX update modes are presented. The equations used in the IDD update mode are presented in reference 2.

In the TCV navigation system the same position-estimate calculations, described in the next section, were used regardless of the position-update mode used to determine the north and east components.

Position Estimate

The first step in the position-estimate process was to develop a velocity-estimate update from the position update:

$$\Delta V_{N,t} = \Delta V_{N,t-1} + K_2 \, \Delta P_{N,t}$$

$$\Delta V_{E,t} = \Delta V_{E,t-1} + K_2 \, \Delta P_{E,t}$$

An updated velocity estimate was then made by summing the velocity update with ground speed obtained from the inertial navigation system:

$$V_{N,t} = \Delta V_{N,t} + \hat{V}_{N,t}$$

$$V_{E,t} = \Delta V_{E,t} + \hat{V}_{E,t}$$

A position update in terms of latitude and longitude was obtained from the system velocity and the position-difference components as follows:

$$\Delta\phi_t = \frac{V_{N,t} \, \Delta t + K_1 \, \Delta P_{N,t}}{r_{M,t}}$$

$$\Delta\lambda_t = \frac{V_{E,t} \, \Delta t + K_1 \, \Delta P_{E,t}}{r_{N,t}}$$

This latitude and longitude position update was based on an oblate-spheroid Earth model (ref. 2) by using the following radii of curvature in the meridional (north/south) and normal (east/west) directions:

$$r_{M,t} = h_{a/p,t} + r_E(1 - 2F + 3F \sin^2 \phi_{e,t-1})$$

$$r_{N,t} = \left[h_{a/p,t} + r_E(1 + F \sin^2 \phi_{e,t-1}) \right] \cos \phi_{e,t-1}$$

The updated position estimate was found by summing the previous position estimate with the position-update terms:

$$\phi_{e,t} = \phi_{e,t-1} + \Delta\phi_t$$

$$\lambda_{e,t} = \lambda_{e,t-1} + \Delta\lambda_t$$

Dual DME (IDD) Position Estimate

Dual DME updating is the normal position update mode. The equations used to determine position difference while in this mode are given in reference 2.

Back-Azimuth/DME (IBD) Position Estimate

General solution.- Figure 4 shows the geometry of the MLS back-azimuth antenna, the DME antenna, the position estimate of the airplane, its position measured with back-azimuth and DME information, and the runway with an extended center line. An orthogonal coordinate system, with its origin placed on the back-azimuth antenna is oriented with respect to true north. Since the DME could be selected either manually or automatically, the position-update equations were derived so that the DME was not required to be colocated with the back-azimuth antenna.

By determining the relative geometry between the back-azimuth antenna, the DME antenna, and the position of the airplane measured with the back-azimuth and DME information, the vector $\vec{z}_{m,t}$ between the origin and the measured position of the airplane was found. The vector $\vec{z}_{e,t-1}$ between the origin and the previously estimated position of the airplane could be found directly from their known latitudes and longitudes. The position difference was then found by subtracting $\vec{z}_{m,t}$ from $\vec{z}_{e,t-1}$.

Calculation of the airplane position vector $\vec{z}_{m,t}$.- Figure 4 shows that $\vec{z}_{m,t}$ is one side of the triangle formed by the origin (back-azimuth antenna), the measured position of the airplane, and the DME antenna. Known quantities used to determine $\vec{z}_{m,t}$ in this triangle include the runway heading ψ_r, the slant range of the DME D'_t, the back-azimuth angle relative to the runway center line η, the location (latitude and longitude) of the DME antenna ϕ_{DME}, λ_{DME}, and the back-azimuth antenna location ϕ_o, λ_o.

Figure 5 shows the angular geometry and distance A between the origin and the DME antenna. The length A and the angle between the DME antenna from the north axis μ remained constant for a particular DME and were calculated only once. If a different DME was tuned, then A and μ were recalculated. The length of A in nautical miles was determined by vectorially summing its components, a and b:

$$a = (\lambda_{DME} - \lambda_o)(60) \cos\left(\frac{\phi_o + \phi_{DME}}{2}\right)$$

$$b = (\phi_{DME} - \phi_o)(60)$$

$$A = \sqrt{a^2 + b^2}$$

The angle μ was found by

$$\mu = \tan^{-1}\left(\frac{a}{b}\right) \qquad (0 \leq \mu \leq 2\pi)$$

The angle α, formed by side A and vector $\vec{z}_{m,t}$ may vary continuously and was calculated 20 times per second. It ranged between 0 and π, inclusive, and was found from

$$\alpha_t = |2\pi - \mu + (\psi_r - \eta_t)|$$

If this calculated value of α_t was greater than π, then

$$\alpha_t = \left|2\pi - \left[|2\pi - \mu + (\psi_r - \eta_t)|\right]\right|$$

The magnitude of the DME reading D'_t, measured in the airplane, was the slant range distance between the ground-based DME antenna and the airplane.

This distance was slant-range-corrected to determine the ground distance D_t between the airplane and DME

$$D_t = D_t' \sin \left[\cos^{-1} \left(\frac{h_{a/p,t} - h_{DME}}{D'} \right) \right]$$

Angle P, formed by the vector $\vec{Z}_{m,t}$ and side D_t, could vary continuously and was calculated 20 times per second. From the relation,

$$\frac{A}{\sin P_t} = \frac{D_t}{\sin \alpha_t}$$

angle P_t was determined from

$$P_t = \sin^{-1} \left(\frac{A}{D_t} \sin \alpha_t \right)$$

Comparison of the square of side A with the sum of the square of side D_t and the square of the magnitude of the vector $Z_{e,t-1}$ (estimated airplane position vector) determined whether angle P_t was obtuse or acute. Hence,

$$P_t = \begin{cases} \sin^{-1} \left(\frac{A}{D_t} \sin \alpha_t \right) & \text{if } A^2 \leq D_t^2 + Z_{e,t-1}^2 \\ \pi - \sin^{-1} \left(\frac{A}{D_t} \sin \alpha_t \right) & \text{if } A^2 > D_t^2 + Z_{e,t-1}^2 \end{cases}$$

The magnitude of the estimated airplane position vector $\vec{Z}_{e,t-1}$ was used as an approximation for $\vec{Z}_{m,t}$. The magnitude of $\vec{Z}_{e,t-1}$ was

$$Z_{e,t-1} = \sqrt{(Z_{e,N,t-1})^2 + (Z_{e,E,t-1})^2}$$

in which

$$Z_{e,N,t-1} = (\phi_{e,t-1} - \phi_o)(60)$$

$$Z_{e,E,t-1} = (\lambda_{e,t-1} - \lambda_o)(60) \cos\left(\frac{\phi_o + \phi_{e,t-1}}{2}\right)$$

The actual magnitude of $\vec{Z}_{m,t}$ was found from

$$Z_{m,t} = A \cos \alpha_t + D_t \cos P_t$$

The north and east components of $\vec{Z}_{m,t}$ were calculated from the angle $\psi_r - \eta_t$ between the north axis and $\vec{Z}_{m,t}$:

$$Z_{m,N,t} = Z_{m,t} \cos (\psi_r - \eta_t)$$

$$Z_{m,E,t} = Z_{m,t} \sin (\psi_r - \eta_t)$$

Calculation of the position difference in north and east components $\Delta P_{N,t}$, $\Delta P_{E,t}$ — IBD update mode.- The position difference in north and east components was now found by subtracting the north component of $\vec{Z}_{e,t-1}$ from the north component of $\vec{Z}_{m,t}$ and by subtracting the east component of $\vec{Z}_{e,t-1}$ from the east component of $\vec{Z}_{m,t}$:

$$\Delta P_{N,t} = Z_{e,N,t-1} - Z_{m,N,t}$$

$$\Delta P_{E,t} = Z_{e,E,t-1} - Z_{m,E,t}$$

These position difference components were then used directly in the navigation position-estimate algorithms.

Back-Azimuth Only (IBX) Position Estimate

General solution.- In the event that a valid DME signal could not be obtained, the navigation computer utilized the back-azimuth signal and inertial velocity to determine a position estimate. Figure 6 shows the geometry of the back-azimuth antenna, the position estimate of the airplane, its estimated position on a measured back-azimuth radial, and the runway with an extended center line. An orthogonal coordinate system, with its origin at the back-azimuth antenna (ϕ_o,λ_o), is oriented in a true-north direction.

Since no DME information was available, no radio position difference could be developed along a radial from the back-azimuth antenna. However, inertial velocity was utilized in the radial direction to supply inputs for a new position estimate in the position-estimate algorithms. Radio position difference in the IBX update mode was limited to a direction perpendicular to the runway center line.

North and east position estimates were found in the following manner. A position-difference vector $\overrightarrow{DP}_t$ was found by subtracting the estimated position vector $\vec{Z}_{e,t-1}$ from the estimated position vector $\vec{Z}_{r,t}$ on the measured back-azimuth angle. The component of $\overrightarrow{DP}_t$ perpendicular to the runway was found and broken into north and east components. These components were used in the navigation position-estimate algorithms. This process was repeated 20 times per second.

Calculation of $\overrightarrow{DP}_t$.- To determine $\overrightarrow{DP}_t$ it was necessary to calculate the position-estimate vector $\vec{Z}_{e,t-1}$ in north and east components from the latitudes and longitudes of the last position estimate and of the back-azimuth antenna location:

$$Z_{e,N,t-1} = (60)(\phi_{e,t-1} - \phi_o)$$

$$Z_{e,E,t-1} = (60)(\lambda_{e,t-1} - \lambda_o)\cos\left(\frac{\phi_{e,t-1} + \phi_o}{2}\right)$$

$$\vec{Z}_{e,t-1} = (Z_{e,E,t-1})\hat{i} + (Z_{e,N,t-1})\hat{j}$$

A vector $\vec{Z}_{r,t}$ of the estimated position of the airplane along a measured back-azimuth radial was determined in the following manner. Since no radio updates could be obtained along a radial from the back-azimuth antenna, it was assumed that the estimated radial distance from the origin was correct. Hence,

the vector lengths of $\vec{Z}_{r,t}$ and $\vec{Z}_{e,t-1}$ were the same (directions could differ to obtain $\overrightarrow{DP}_t$). The length of $\vec{Z}_{r,t}$ and $\vec{Z}_{e,t-1}$ was

$$Z_{r,t} = Z_{e,t-1} = \sqrt{(Z_{e,N,t-1})^2 + (Z_{e,E,t-1})^2}$$

The north and east components of $\vec{Z}_{r,t}$ were found from the angle $\psi_r - \eta_t$ between the vector $\vec{Z}_{r,t}$ and the north axis:

$$Z_{r,N,t} = Z_{r,t} \cos (\psi_r - \eta_t)$$

$$Z_{r,E,t} = Z_{r,t} \sin (\psi_r - \eta_t)$$

$$\vec{Z}_{r,t} = (Z_{r,E,t})\hat{i} + (Z_{r,N,t})\hat{j}$$

$\overrightarrow{DP}_t$ was found vectorially:

$$\overrightarrow{DP}_t = \vec{Z}_{r,t} - \vec{Z}_{e,t-1}$$

Calculation of the position difference $\Delta P_{N,t}$, $\Delta P_{E,t}$ - IBX update mode.- The magnitude of the component of $\overrightarrow{DP}_t$ perpendicular to the runway center line was obtained by the dot product of $\overrightarrow{DP}_t$ and a unit vector $\hat{u}$ perpendicular to the runway center line. The unit vector $\hat{u}$, shown in figure 6, was

$$\hat{u} = -\cos (\psi_r)\hat{i} + \sin (\psi_r)\hat{j}$$

The magnitude of $\overrightarrow{DP}_{p,t}$ was thus

$$DP_{p,t} = \overrightarrow{DP}_t \cdot \hat{u}$$

$$= -(Z_{r,E,t} - Z_{e,E,t-1}) \cos \psi_r + (Z_{r,N,t} - Z_{e,N,t-1}) \sin \phi_r$$

This provided the magnitude of the position difference. The north and east components of the position difference were

$$\Delta P_{N,t} = DP_{p,t} \sin \psi_r$$

$$\Delta P_{E,t} = -DP_{p,t} \cos \psi_r$$

These position-difference components were used directly in the navigation position-estimate algorithms.

Back-Azimuth/Airplane Position Validity Check

Since random DME selection, automatic frequency tuning, and other means of automatic software control were utilized in the navigation computer, a check had to be made to ensure that the navigation computer was using the appropriate navigation data for the area in which the airplane was flying. Obviously, if improper navigation data were being utilized, position estimates based on those data would be inaccurate and should not be used.

To preclude the use of the wrong MLS back-azimuth navigation data, a volumetric geometric check was made to determine whether the position estimate of the airplane was within the MLS back-azimuth boundaries. If the airplane was not within these boundaries, then MLS updating was inhibited. These boundaries included lateral and radial limits of coverage as shown in figure 7. The lateral limit of the back-azimuth angle of coverage is $\pm\omega$ from the runway center line. Radial limits required that the airplane be within a distance L in meters (n. mi) of the back-azimuth antenna, but not closer than a distance M in meters (n. mi). A vertical angle of coverage limit Ω was measured from the back-azimuth antenna.

A new orthogonal coordinate system, with its origin located at the back-azimuth antenna and its X'-axis parallel to the runway center line, was used to make the geometric check. The north and east components of the estimated position vector $\vec{Z}_{e,t-1}$ were transformed into the new X',Y' coordinate system as follows:

$$X'_{e,t} = Z_{e,N,t-1} \cos \psi_r + Z_{e,E,t-1} \sin \psi_r$$

$$Y'_{e,t} = Z_{e,N,t-1} \sin \psi_r - Z_{e,E,t-1} \cos \psi_r$$

The lateral azimuth check was then

$$-X'_{e,t} \tan \omega \leq Y'_{e,t} \leq X'_{e,t} \tan \omega$$

The radial check was

$$M \leqq \frac{x'_{e,t}}{\cos \eta_t} \leqq L$$

The vertical check was

$$h_{a/p,t} \leqq h_o + x'_{e,t} \tan \Omega$$

For these tests, the MLS back-azimuth coverage limits were

Lateral	$\omega = \pm 42^o$
Vertical	$\Omega = 20^o$
Inner radial	M = 3048 m
Outer radial	L = 37 040 m (20 n. mi.)

RESULTS AND DISCUSSION

Flight data were gathered on a total of 43 test runs along path 2 and path 3 and on the return flight to the start of path 1. Position-estimate updates were accomplished on 27 update segments in the IBD mode, 7 update segments in the IBX mode, and 30 update segments in the IDD mode. Typically, segments lasted between 1 and 4 minutes. Position estimates from the navigation system in each update mode were compared with radar data to obtain the position-estimate error vector. The mean and standard deviation of the magnitude and direction of this vector were determined for each update mode.

IBD Update Mode

In the IBD mode, the magnitude of the position-estimate error vector had a mean of 124.3 m and a standard deviation of 60 m. The mean direction of the error vector was 298.1^o with a standard deviation of 35.7^o.

Figure 8 shows how the position-estimate error vector is divided into two components, so that the errors due to the back-azimuth signal input and by the DME signal input can be separated. The first component e_p is perpendicular to the back-azimuth radial on which the airplane is located. The e_p component is influenced by the back-azimuth signal input. The second component e_R is a radial error along the back-azimuth radial on which the airplane is located. The e_R component is influenced primarily by the DME signal input and to a lesser extent by the back-azimuth signal. The e_R component increases linearly as a function of the range R from the back-azimuth antenna to the airplane if the azimuth bearing error e_θ (fig. 8) is constant (i.e., $e_p = Re_\theta$).

Figure 9 shows the e_p component as a function of R for selected points from flights along the zero back-azimuth radial. These data are grouped about a straight line with a slope representing a constant $e_\theta = 0.05^o$. To determine how the e_p component varied on other back-azimuth radials, data were used from flights along two other path segments. The first path segment was the last leg of path 3 which diverged from the runway center line at a 45^o angle. The second path segment was parallel to the runway center line, but offset by 6100 m. This path segment was flown back toward the runway. These paths provided data at various ranges for all back-azimuth radials on the left-hand side of the azimuth coverage. (Flight during the test period was confined to this side of MLS coverage due to air-traffic-control considerations.)

Figure 10 shows the e_p component as a function of range from the back-azimuth antenna during flight along these path segments. The data lie above the line representing a constant $e_\theta = 0.05^o$. Therefore, e_θ was larger for azimuth radials which were not on the runway center line.

To determine how position error varied for different back-azimuth radials, the e_p component from all flights (including those along the zero-azimuth radial) was normalized for range effects and plotted in the form of e_θ as a function of the back-azimuth radial. Figure 11 shows that these data were grouped about a straight line drawn from $e_\theta = 0.05^o$ at the zero-azimuth radial to $e_\theta = 0.28^o$ at the 40^o radial. The straight line in figure 11 shows the expected e_θ error as a function of the back-azimuth radial. An expected e_p component can be found by multiplying the range from the back-azimuth antenna and the appropriate e_θ obtained from the straight line.

The radial component of error e_R was plotted as a function of range from the back-azimuth antenna in figure 12. The e_R components for flights on both path 2 and path 3 are randomly grouped about a mean value of 120 m. The figure shows that the e_R component did not vary significantly with range.

The e_R component contributed the most to the navigation position-estimate error. The e_p component contributed a smaller error that varied as a function of the back-azimuth radial and the range from the back-azimuth antenna. The expected e_p component was shown to be less than 32 m within a range of 37 040 m (20 n. mi.) from the back-azimuth antenna. For operations off the zero-azimuth radial, the e_p component will become as large as the e_R component only when the airplane is close to the lateral limits of the back-azimuth coverage and at large distances from the back-azimuth antenna.

The DME ground station used during these flight tests was a standard DME station used for normal en route navigation. The expected accuracy of these stations is about 185 m (ref. 6). A reduction of the DME ground-station error, which could be obtained with a PDME, could reduce the radial component of error and result in an improved navigation position estimate during the IBD update mode.

IBX Update Mode

In the IBX update mode, the magnitude of the position-estimate error vector had a mean of 145.3 m and a standard deviation of 71.3 m. The mean and standard deviation for the direction of the position-estimate error vector was not summarized since radio position updating does not occur omnidirectionally in this mode.

Both the magnitude and direction of the position-estimate error vector were strongly dependent upon the initial error when the IBX update mode started. Corrections to the position estimate were made only in a direction perpendicular to the back-azimuth radial on which the airplane was located. No corrections could be made in a radial direction since DME signal inputs were not available.

Figure 13 shows the e_p and e_R error components for a flight along the zero-azimuth radial. The IBX update mode was started with initial navigation position-estimate errors of $e_p = 140$ m and $e_R = 118$ m. The e_p component was reduced because of back-azimuth signal inputs but the e_R component remained virtually unchanged since no DME signal inputs were available.

Figure 14 shows the e_p component as a function of range when the airplane was flown along path 2 and back to the start of path 1. The results were similar to those obtained in the IBD update mode: $e_\theta = 0.05^\circ$ on the zero-azimuth bearing and $e_\theta \leq 0.25^\circ$ on the return leg.

IDD Update Mode

In the IDD update mode, the position-estimate error vector was random in direction and had a mean magnitude of 183.5 m and a standard deviation of 81.1 m. These results are within the 185-m accuracy tolerance for DME ground stations and are similar to past experience with the dual DME update mode (ref. 5). It is expected that the use of PDME inputs also could improve the position-estimate accuracy in the IDD update mode.

CONCLUDING REMARKS

Flight tests with the NASA Terminal Configured Vehicle (TCV) Boeing 737-100 airplane in the time-referenced scanning-beam (TRSB) microwave landing-system (MLS) environment have shown that the accuracy of position estimates based on dual distance-measuring-equipment (DME) inputs can be improved by using MLS back-azimuth radio signals. Position estimates from a combination of back-azimuth and DME signals achieved the best position-estimate accuracy. The next best accuracy was obtained from back-azimuth signals alone. The least accurate update mode of the three tested was the dual DME mode.

The position-estimate accuracy was established by computing an error vector between the position of the airplane defined by ground-based radar tracking and the airplane position estimated by the airplane navigation system. This error vector was divided into two components: a component perpendicular

to the back-azimuth bearing, influenced by back-azimuth signal inputs; and a component parallel to the back-azimuth bearings, influenced primarily by the DME signal inputs.

For updates using both DME and back-azimuth signal inputs, the radial component of error contributed the largest portion to the error vector. The radial component of error was generally constant as a function of range from the back-azimuth antenna and was within accuracy tolerances for this DME station. The DME ground station used during these tests was a standard en route navigation station. The use of a precision DME ground station probably could improve the accuracy of the position estimate.

The perpendicular component of error was influenced both by range from the back-azimuth antenna and by the particular back-azimuth radial on which the airplane was located.

For updates which used only the back-azimuth signal inputs, position-estimate error was strongly dependent upon the initial position-estimate error since corrections were made only in the perpendicular direction. The perpendicular component of error showed accuracy characteristics similar to those observed during updates using both DME and back-azimuth inputs.

For updates which used dual DME, position-estimate error was within the accuracy tolerance specified for en route DME and was similar to previous experience with dual DME updating. The accuracy of the position estimate could be improved with the use of precision DME signal inputs.

Langley Research Center
National Aeronautics and Space Administration
Hampton, VA 23665
November 13, 1979

REFERENCES

1. Walsh, Thomas M.; and Weener, Earl F.: Automatic Flight Performance of a Transport Airplane on Complex Microwave Landing System Paths. NASA Paper presented at AGARD 25th GCP Symposium on Guidance and Control Design Considerations for Low Altitude and Terminal Area Flight (Dayton, Ohio), Oct. 1977.

2. Cosley, D.; and Martin, A. J.: ADEDS Functional/Software Requirements. SST Technology Follow-On Program - Phase II. Rep. No. FAA-SS-73-19, Dec. 1973. (Available from DDC as AD B000 287.)

3. McKinstry, R. Gill: Guidance Algorithms and Non-Critical Control Laws for ADEDS and the AGCS Model NASA 515. Doc. D6-41565, Boeing Co., 1974.

4. Microwave Landing System Phase II Tracker Error Study. FAA Report No. FAA-RD-74-207, Dec. 1974.

5. Knox, Charles E.: Experimental Determination of the Navigation Error of the 4-D Navigation, Guidance, and Control Systems on the NASA B-737 Airplane. NASA Paper presented at AGARD 25th GCP Symposium on Guidance and Control Design Considerations for Low Altitude and Terminal Area Flight (Dayton, Ohio), Oct. 1977.

6. Approval of Area Navigation Systems for Use in the U.S. National Airspace System. AC No. 90-45A, FAA, Feb. 21, 1975.

L-73-6281

Figure 1.- NASA terminal configured vehicle (TCV) research airplane.

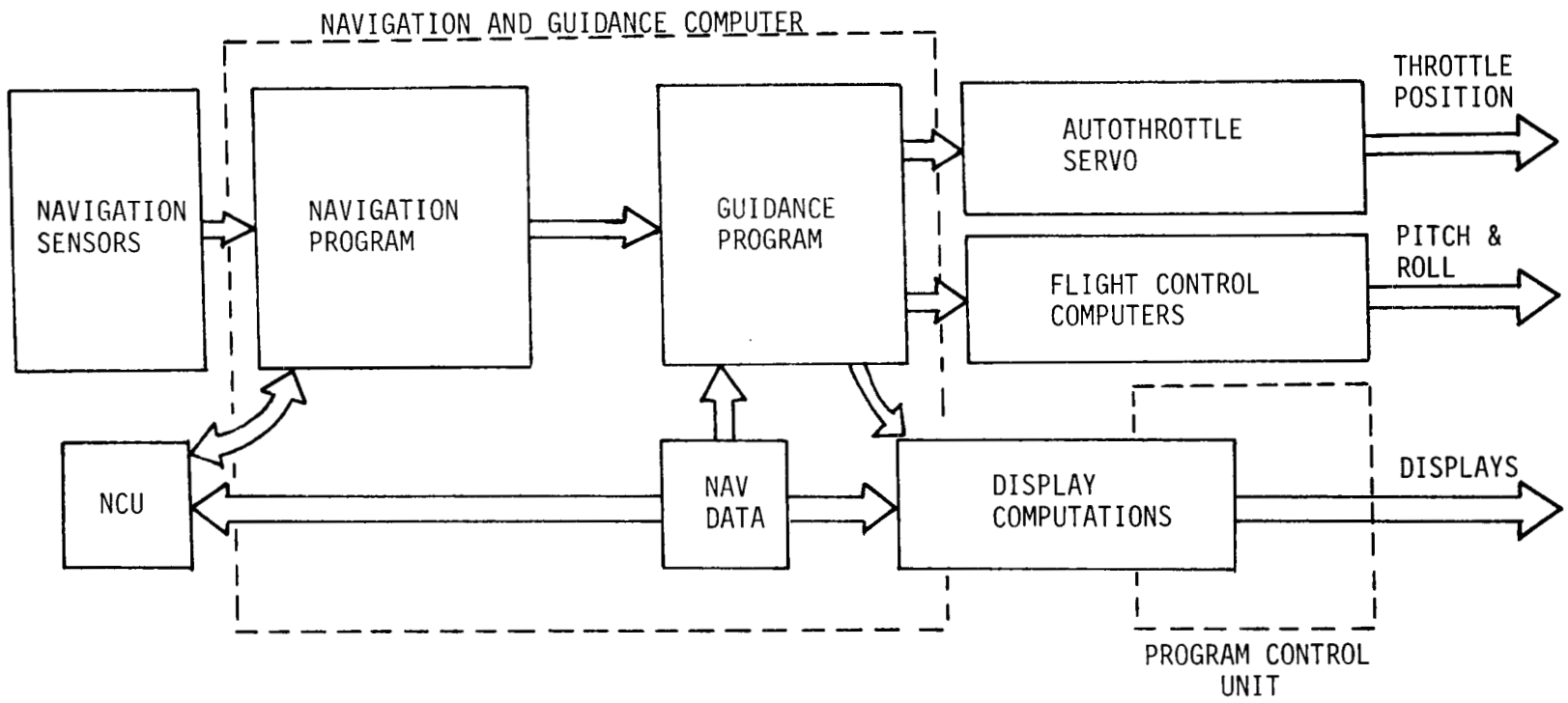

Figure 2.- Functional block diagram of navigation, guidance, and control systems.

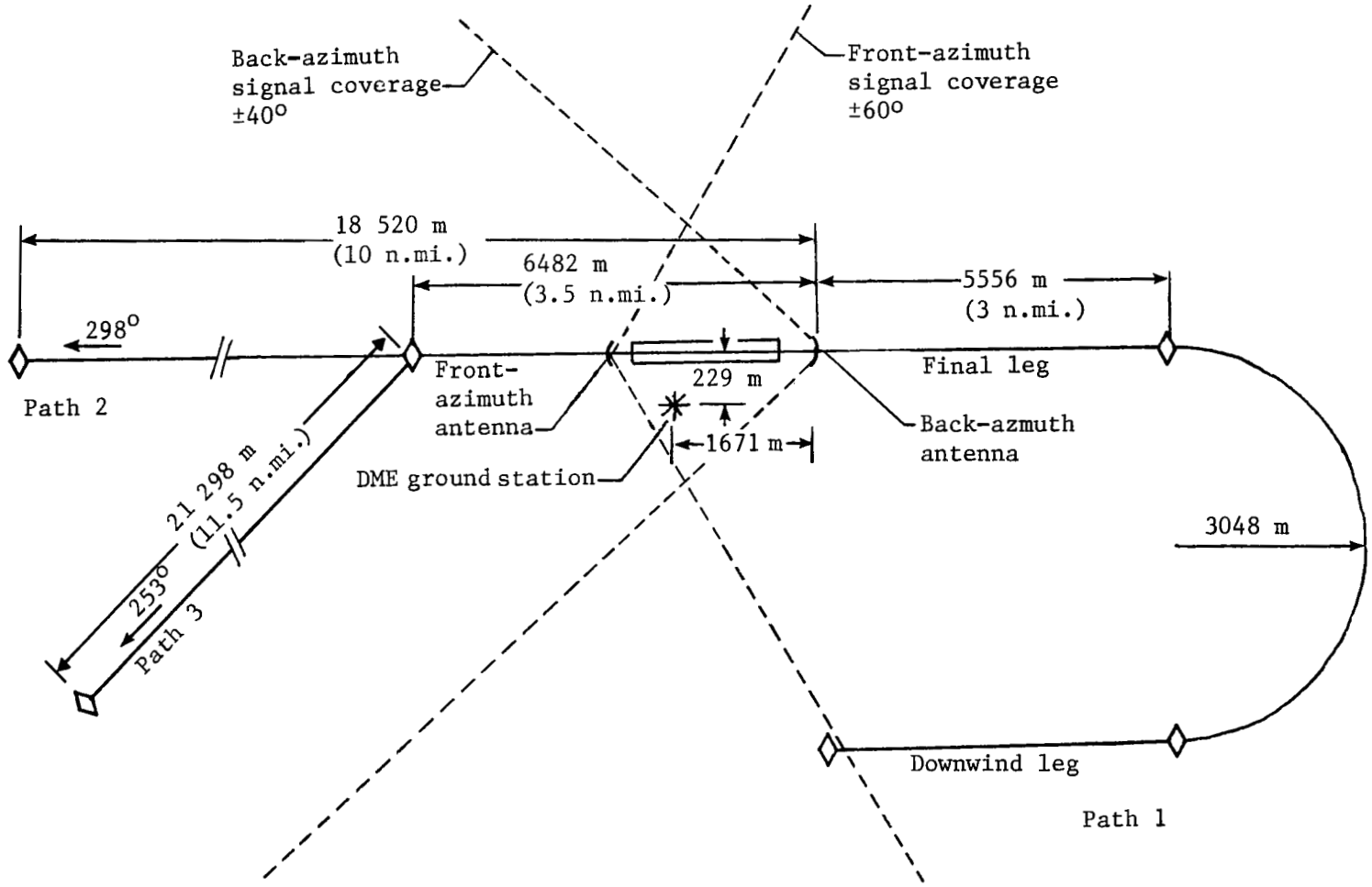

Figure 3.- Flight test paths within the MLS front- and back-azimuth signal coverage. Headings are relative to true north.

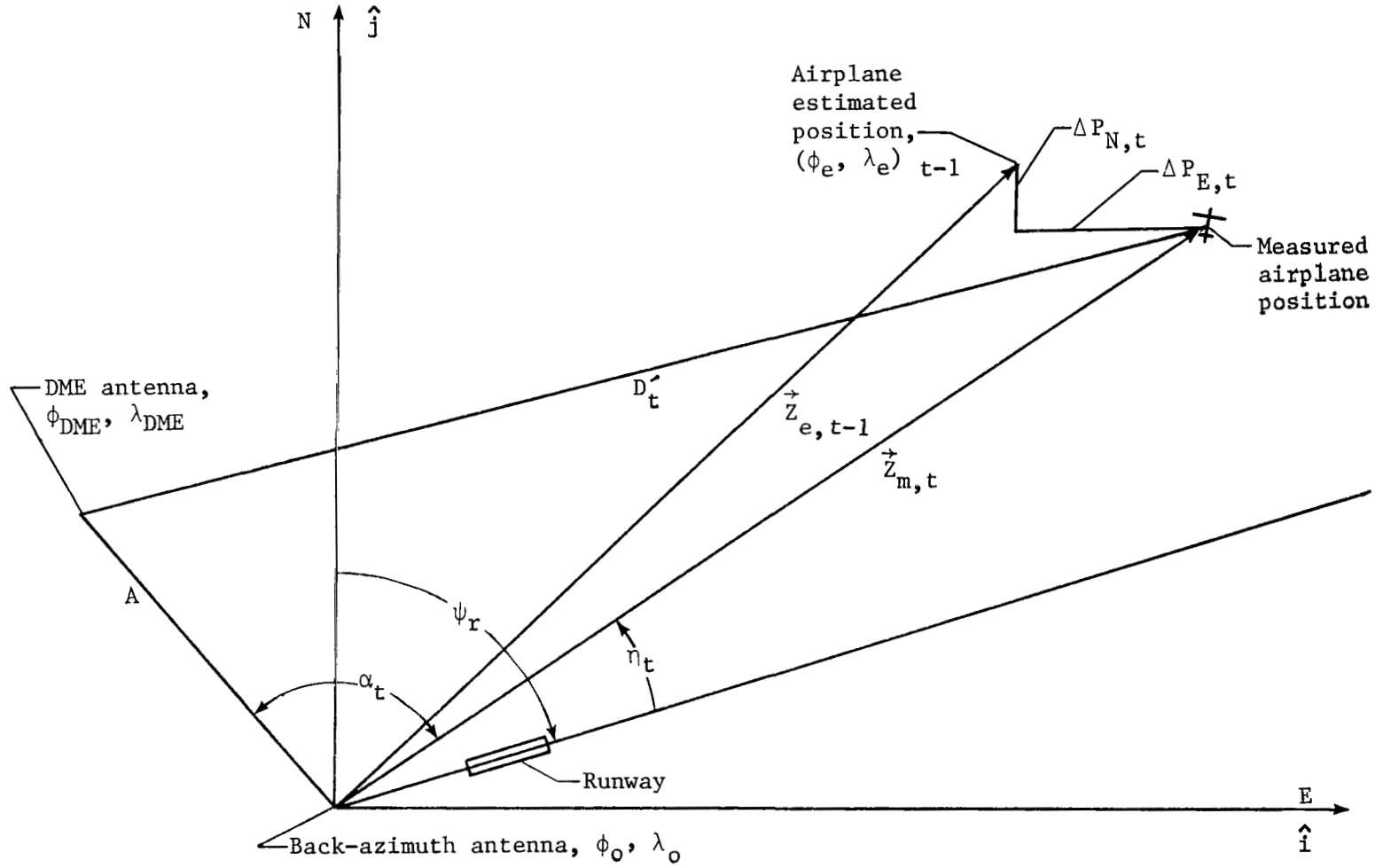

Figure 4.- Geometry pertaining to IBD update mode: back-azimuth antenna, DME, estimated and measured positions of airplane, and runway with extended center line.

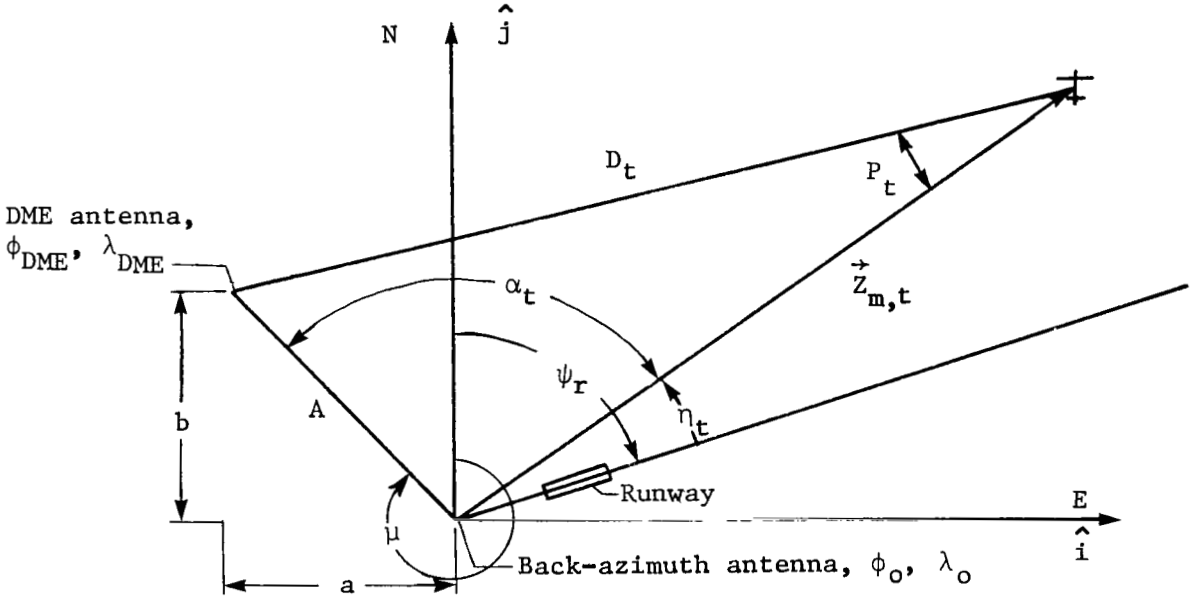

Figure 5.- Vector $\vec{Z}_{m,t}$ triangle components; IBD update mode.

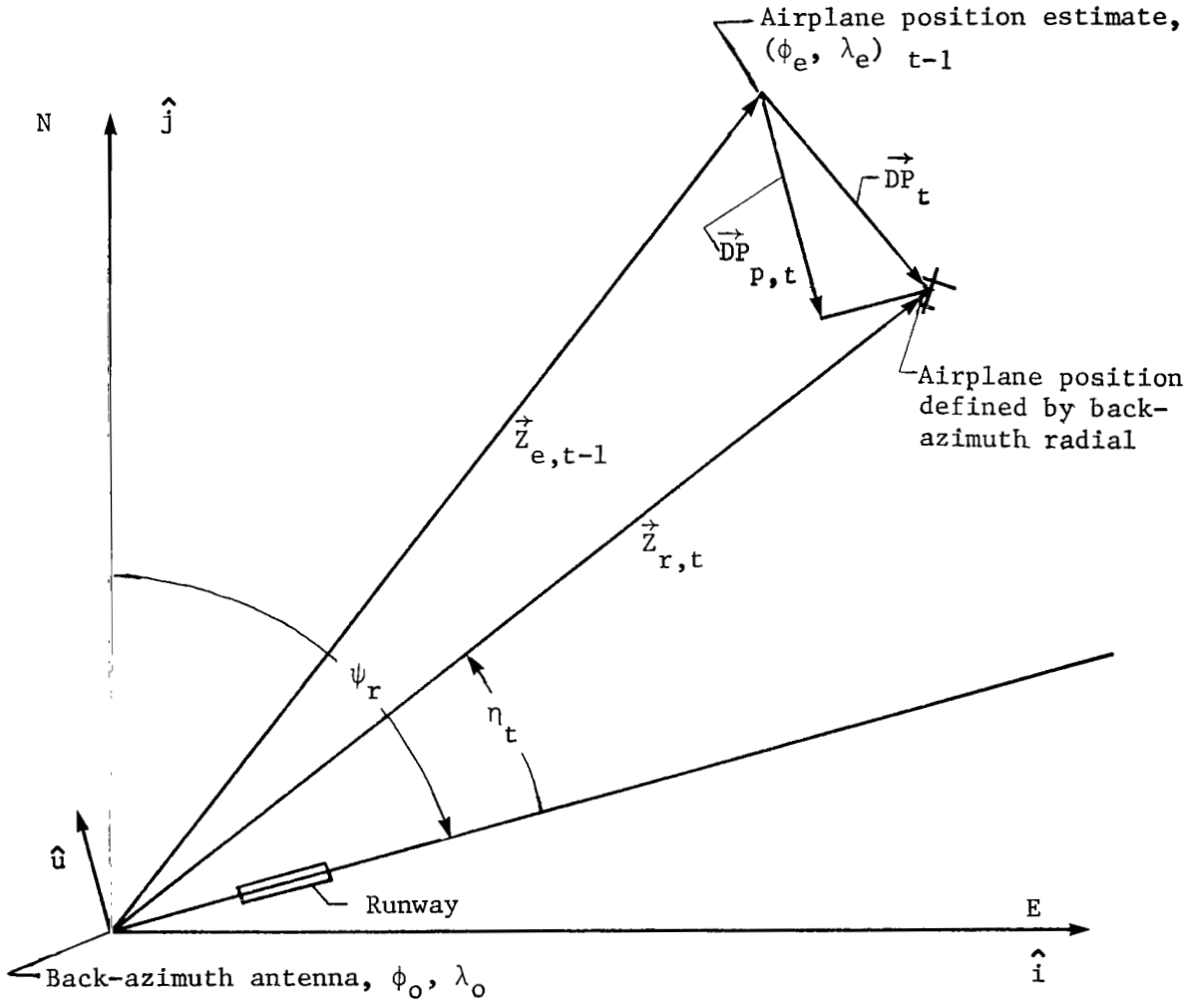

Figure 6.- Geometry pertaining to IBX update mode: back-azimuth antenna location, estimated and measured azimuth positions of airplane, and runway with extended center line.

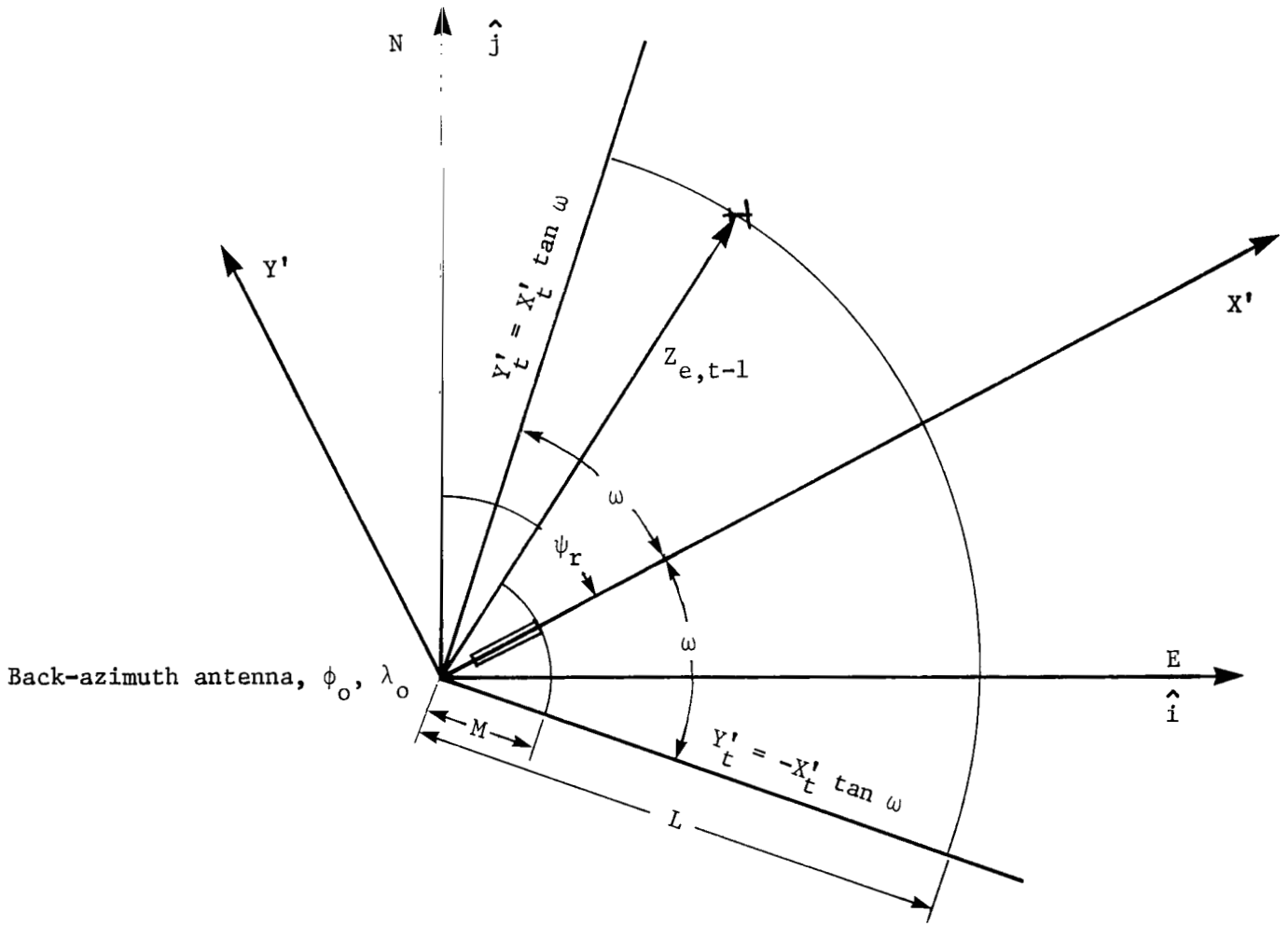

Figure 7.- Lateral and radial MLS back-azimuth geometry limits: ω, L, and M.

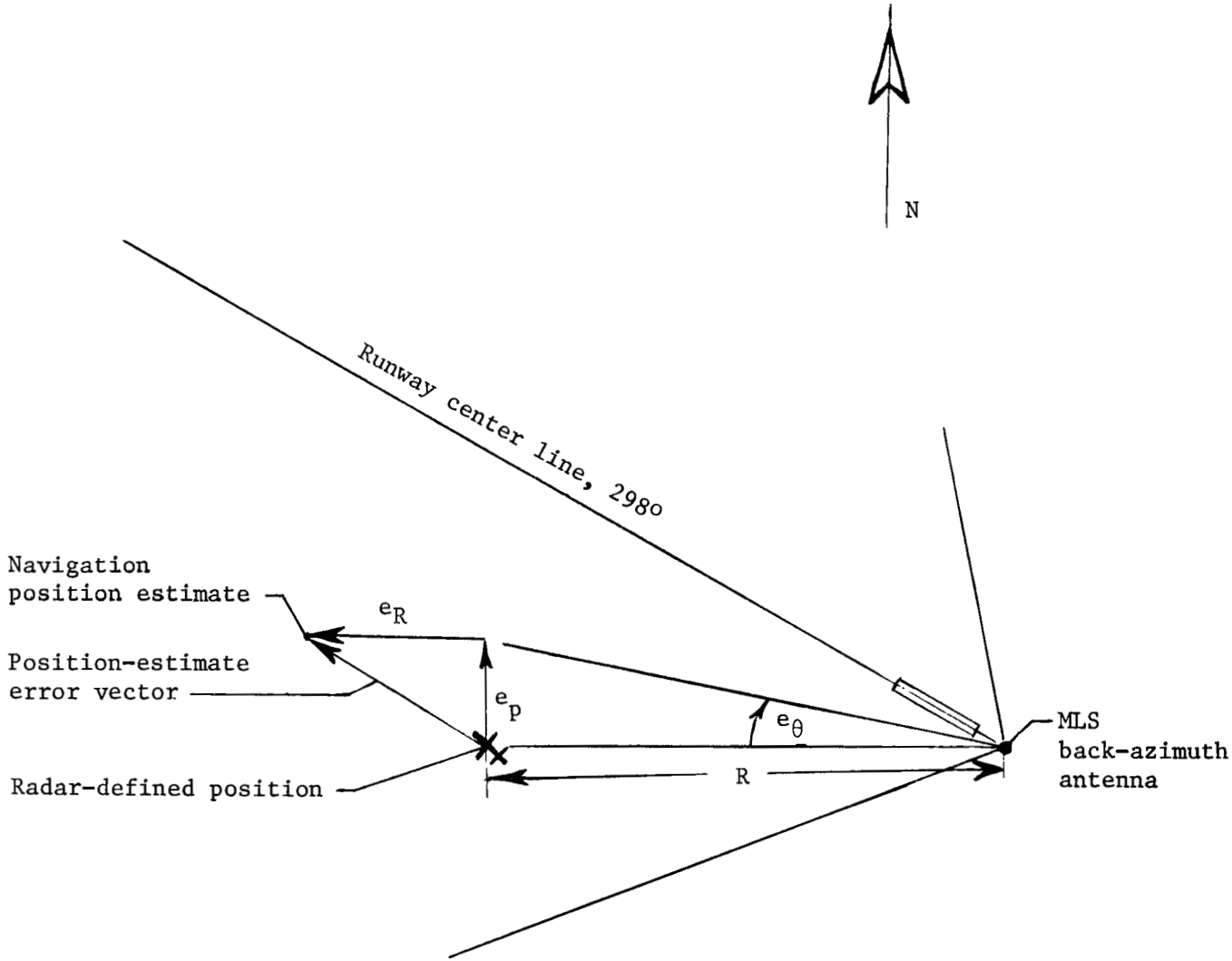

Figure 8.- Perpendicular and radial components of position-estimate error; e_p, e_R, and e_θ are positive as shown.

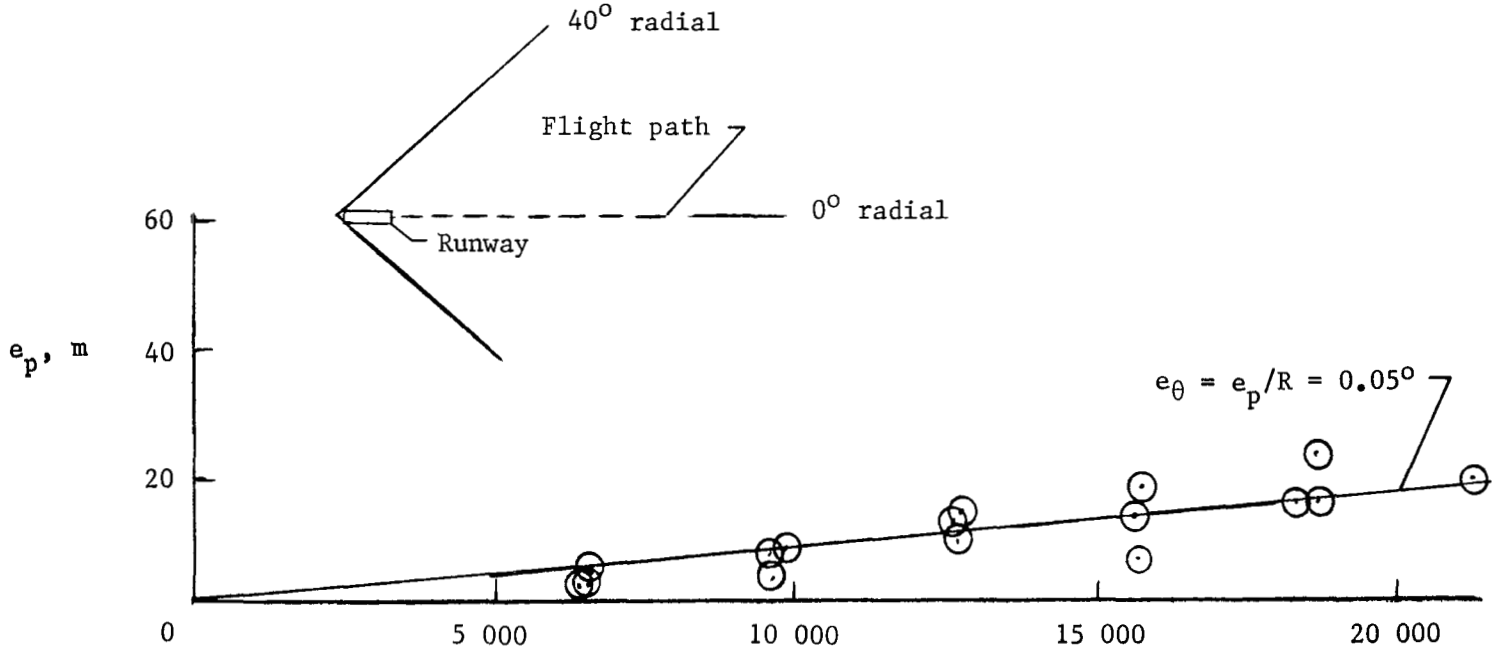

Figure 9.- Perpendicular component of position-estimate error on the zero back-azimuth radial; IBD update mode.

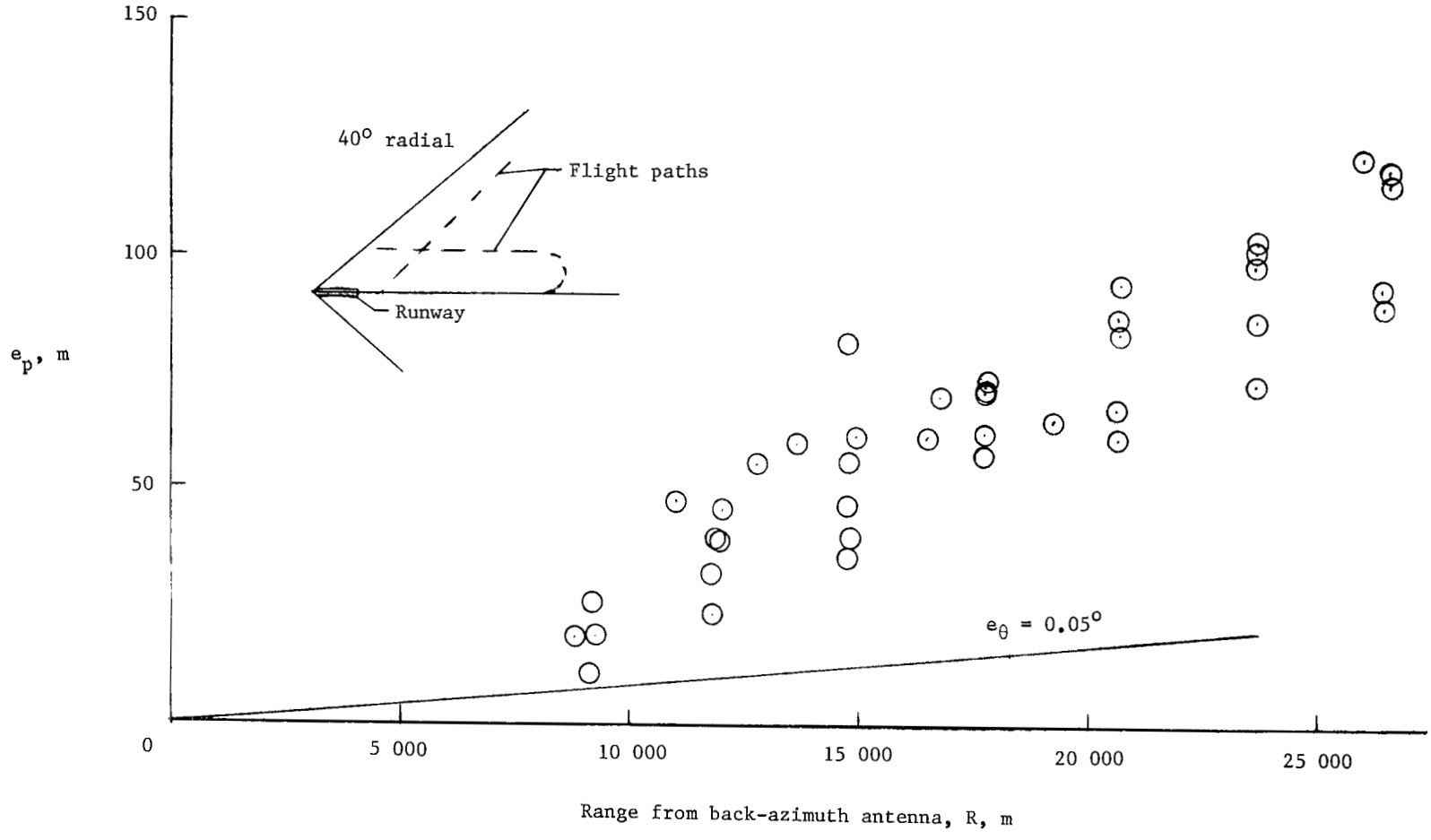

Figure 10.- Perpendicular component of position estimate error on various back-azimuth radials up to 40°; IBD update mode.

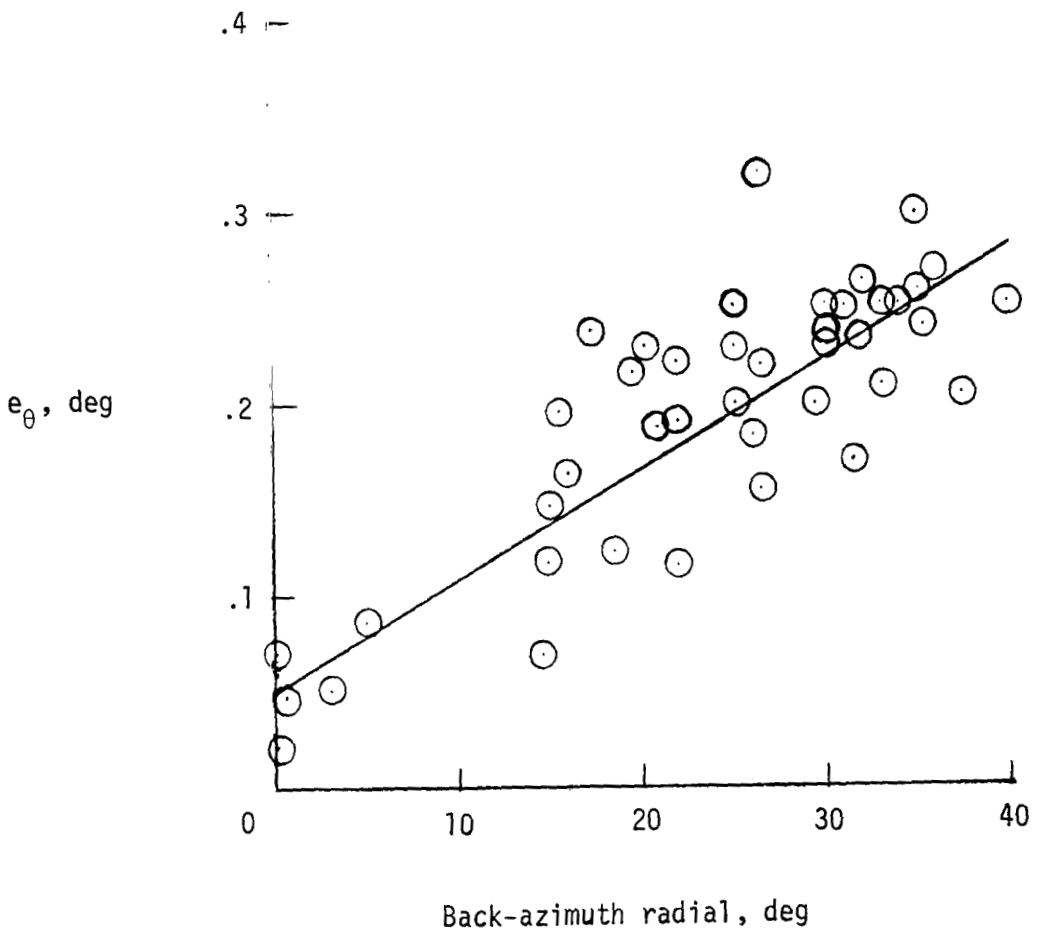

Figure 11.- Perpendicular component of position-estimate error normalized for range R as a function of the back-azimuth radial; IBD update mode.

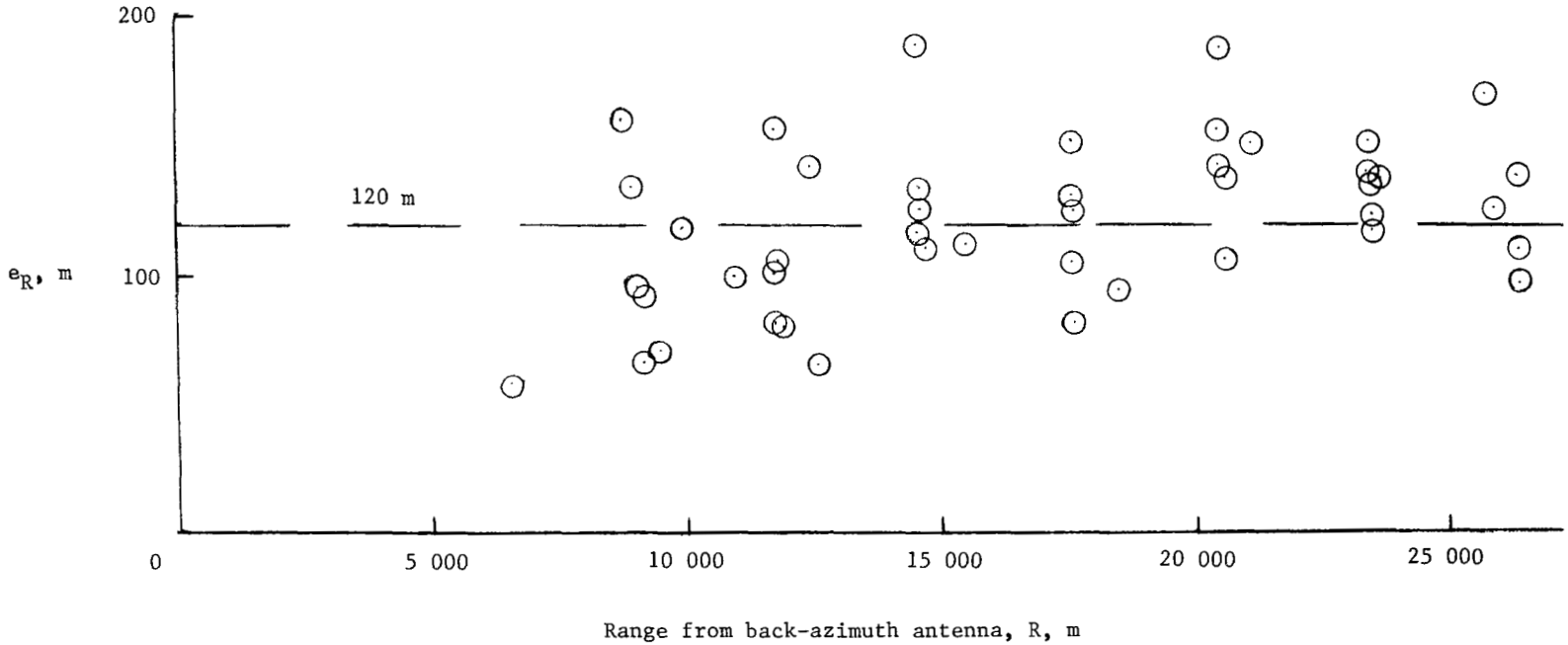

Figure 12.- Radial component of position-estimate error; IBD update mode.

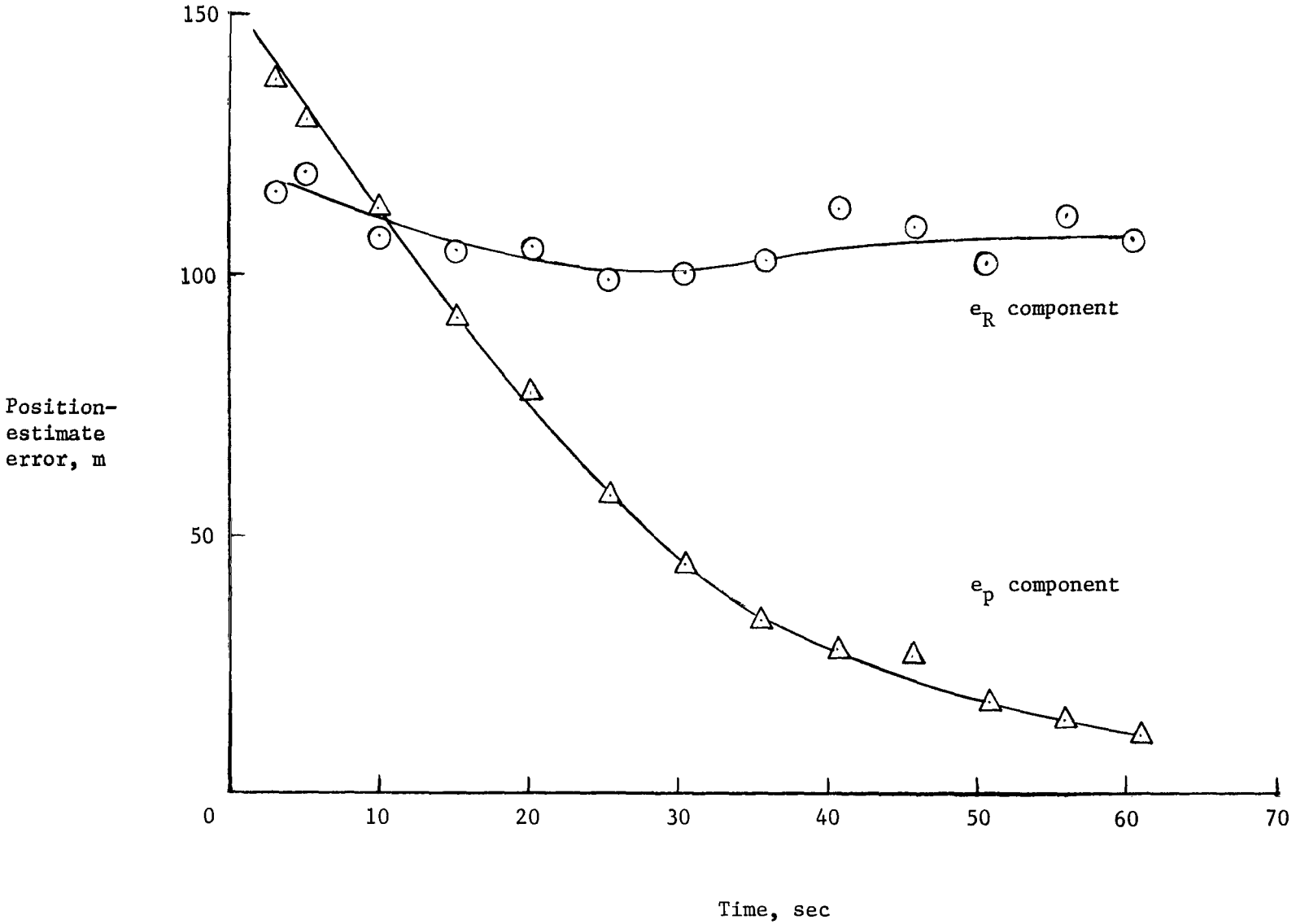

Figure 13.- The e_p and e_R components of position-estimate error from an initial error; IBX update mode.

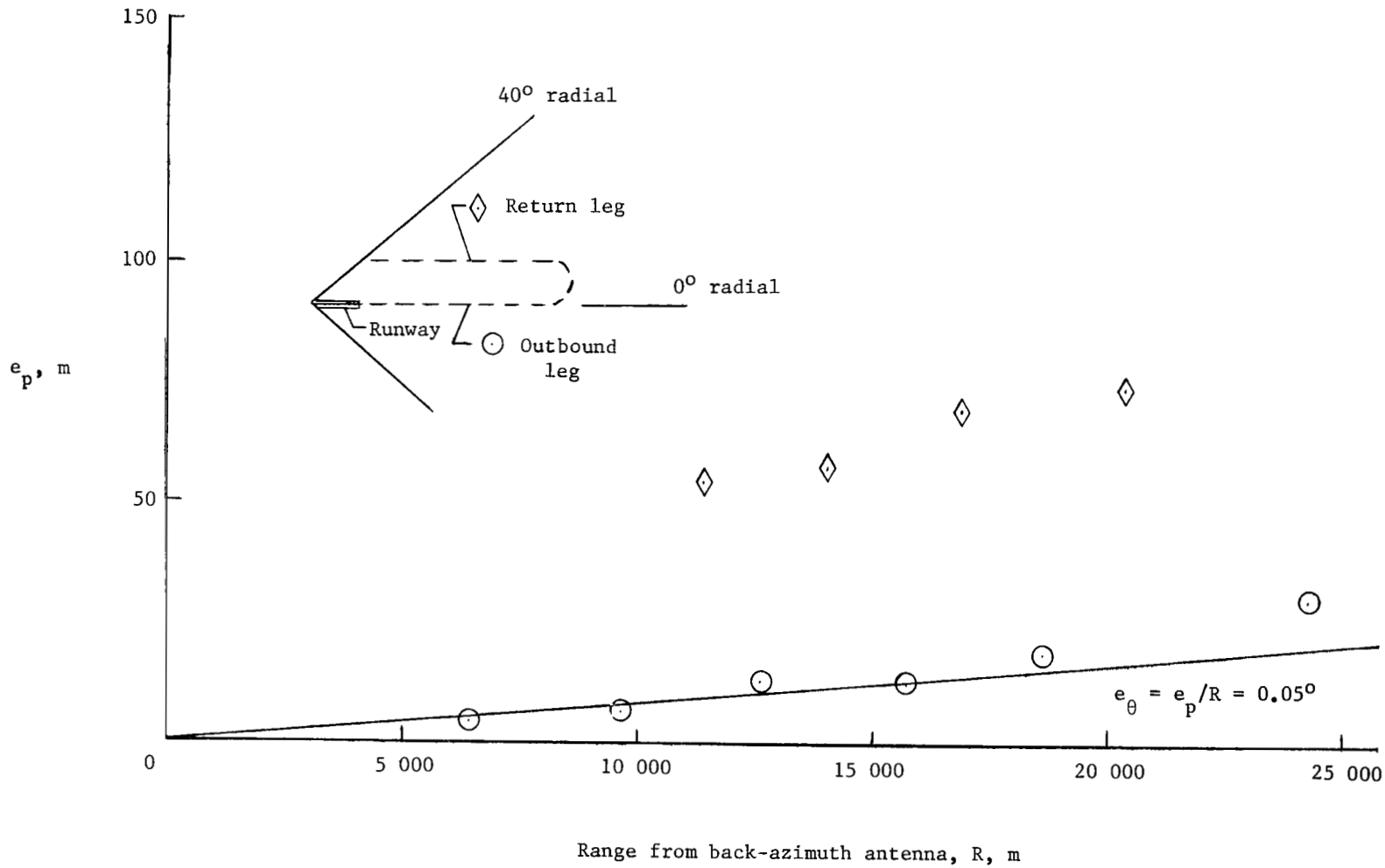

Figure 14.- Perpendicular component of position-estimate error on various back-azimuth radials between 0° and 40°; IBX update mode.

1. Report No.	2. Government Accession No.	3. Recipient's Catalog No.
NASA TP-1574		

4. Title and Subtitle	5. Report Date
EXPERIMENTAL DETERMINATION OF POSITION-ESTIMATE ACCURACY USING BACK-AZIMUTH SIGNALS FROM A MICROWAVE LANDING SYSTEM	December 1979
	6. Performing Organization Code
7. Author(s)	8. Performing Organization Report No.
Charles E. Knox	L-13074
	10. Work Unit No.
9. Performing Organization Name and Address	513-52-13-62
NASA Langley Research Center Hampton, VA 23665	11. Contract or Grant No.
	13. Type of Report and Period Covered
12. Sponsoring Agency Name and Address	Technical Paper
National Aeronautics and Space Administration Washington, DC 20546	14. Sponsoring Agency Code

15. Supplementary Notes

16. Abstract

This paper presents the results of flight tests using the NASA Terminal Configured Vehicle (TCV) Boeing 737 airplane to obtain position estimates with back-azimuth signals from a microwave landing system. The most accurate position estimates were obtained from a combination of back-azimuth and distance-measuring-equipment (DME) signals. Less accurate position estimates were obtained with back-azimuth signals alone; the least accurate position estimates were obtained with dual DME signals.

17. Key Words (Suggested by Author(s))	18. Distribution Statement
Navigation Guidance Microwave landing system	Unclassified - Unlimited Subject Category 04

19. Security Classif. (of this report)	20. Security Classif. (of this page)	21. No. of Pages	22. Price*
Unclassified	Unclassified	34	$4.50

* For sale by the National Technical Information Service, Springfield, Virginia 22161

NASA-Langley, 1979

National Aeronautics and Space Administration

Washington, D.C.
20546

Official Business
Penalty for Private Use, $300

THIRD-CLASS BULK RATE

Postage and Fees Paid
National Aeronautics and
Space Administration
NASA-451

6 1 1U,A, 121779 S00903DS
DEPT OF THE AIR FORCE
AF WEAPONS LABORATORY
ATTN: TECHNICAL LIBRARY (SUL)
KIRTLAND AFB NM 87117

NASA

POSTMASTER: If Undeliverable (Section 158 Postal Manual) Do Not Return